Journal of Solid State Chemistry 181 (2008) 2572–2579

Contents lists available at ScienceDirect

Journal of Solid State Chemistry

journal homepage: www.elsevier.com/locate/jssc

Solid solutions of perovskite in the $LaO_{1.5}$–BaO–$ScO_{1.5}$–ZrO_2 system at 1600 °C

Koichi Suehiro, Susumu Imashuku, Tetsuya Uda *, Yoshitaro Nose, Yasuhiro Awakura

Department of Materials Science and Engineering, Kyoto University, Yoshida-Honmachi, Kyoto 606-8501, Japan

ARTICLE INFO

Article history:
Received 17 January 2008
Received in revised form
2 May 2008
Accepted 7 June 2008
Available online 17 June 2008

Keywords:
Phase diagram
Fuel cell
Solubility
Thermodynamics

ABSTRACT

A partial pseudoternary phase diagram of the $LaO_{1.5}$–BaO–$ScO_{1.5}$ system was established at 1600 °C. According to the phase diagram, the solubility of barium into the cubic perovskite phase ($LaScO_3$) at 1600 °C is 0.24 in a mole fraction of barium oxide (X_{BaO}) on the composition line where the mole fraction of scandium oxide is 0.50. Another cubic perovskite phase ($BaZrO_3$) in the BaO–ZrO_2–$ScO_{1.5}$ system is also known. We investigated the phase relationships between the two cubic perovskites in the pseudoquaternary phase diagram of the $LaO_{1.5}$–BaO–$ScO_{1.5}$–ZrO_2 system. As a result, we found the existence of a wide solid solution region between the cubic perovskites at 1600 °C. The region was determined by X-ray diffraction (XRD) analysis and energy dispersive X-ray (EDX) microanalysis of samples with various compositions, and established the partial pseudoquaternary phase diagram.

1. Introduction

The crystallographic structure of lanthanum scandate ($LaScO_3$) belongs to the perovskite-type, and divalent cation (M(II))-doped lanthanum scandate was reported to be a proton conductive oxide in wet atmosphere [1]. Barium has been reported as a dopant for lanthanum scandate [1]. The 20% barium-doped lanthanum scandate has a cubic perovskite structure in contrast to non-doped lanthanum scandate which has an orthorhombic perovskite structure. The solubility of barium and the structure of doped lanthanum scandate are quite important information for evaluating the protonic conductivity and its basic science. We therefore intended to determine the solubility of BaO into $LaScO_3$ and the relationship between the structure and the amount of doped BaO by establishing the pseudoternary phase diagram of the $LaO_{1.5}$–BaO–$ScO_{1.5}$ system at 1600 °C, which is a typical sintering temperature of lanthanum scandate. A partial phase relationship related to another cubic perovskite phase in the BaO–ZrO_2–$ScO_{1.5}$ system at 1600 °C has been reported [2]. Fig. 1 shows the schematic pseudoquaternary phase diagram with two pseudoternary phase diagrams, although the pseudoternary phase diagram of the $LaO_{1.5}$–BaO–$ScO_{1.5}$ system will be established in this study. In the $LaO_{1.5}$–BaO–$ScO_{1.5}$ pseudoternary system, there is solid solution based on cubic and orthorhombic perovskite-lanthanum scandate ($LaScO_3$). In the BaO–$ScO_{1.5}$–ZrO_2 pseudoternary system, there is another solid solution of cubic perovskite-barium zirconate ($BaZrO_3$). We speculated that there is a solid solution between the cubic lanthanum scandate and barium zirconate. In this case, we assumed that Ba can substitute for only La sites and Sc can substitute for only Zr sites because the ionic radius of Ba (1.61 Å at 12 coordination) is close to that of La (1.36 Å at 12 coordination) rather than that of Sc (0.76 Å at 6 coordination) and the ionic radius of Sc (0.76 Å) is almost the same as that of Zr (0.72 Å at 6 coordination). This assumption means that the following Eq. (1) has to be satisfied:

$$X_{LaO_{1.5}} + X_{BaO} = 0.50$$
$$X_{ScO_{1.5}} + X_{ZrO_2} = 0.50, \quad (1)$$

where X_i is the mole fraction of i. This requirement is identical to a set of points on the cross-section of the pseudoquaternary phase diagram of the $LaO_{1.5}$–BaO–$ScO_{1.5}$–ZrO_2 system in Fig. 1. That is, if such a solid solution exists, the solution must be on the cross-section. We therefore investigated the phase relationship in the cross-section again at the typical sintering temperature of 1600 °C.

2. Experimental

2.1. Chemical analysis and phase identification

The nominal compositions of samples examined in this work are listed in Table 1(a) and (b) with results of phase identification by X-ray diffraction (XRD) analysis (Rigaku Corporation, RINT2200, Cu-$K\alpha$). The compositions of each grain in the samples after heat treatment at 1600 °C for 24 h were analyzed by energy dispersive X-ray microanalysis (EDX) (JEOL, JED-2300) equipped with a field emission-scanning electron microscope (FE-SEM) (JEOL, JSM-6500F). We used fluorescent X-rays of La $L\alpha_1$, Ba $L\alpha_1$, Sc

* Corresponding author.
E-mail address: tetsuya-uda@mtl.kyoto-u.ac.jp (T. Uda).

0022-4596/$ - see front matter © 2008 Elsevier Inc. All rights reserved.
doi:10.1016/j.jssc.2008.06.025

$K\beta_1$ and Sc $K\beta_1$ for analysis. The compositions of each grain in the samples by EDX were calibrated based on the assumption that the average compositions of whole samples analyzed by EDX are equal to the nominal compositions.

2.2. Material preparation

All samples were synthesized by a solid-state reaction from lanthania (La_2O_3: 99.99%, Nacalai Tesque), barium carbonate ($BaCO_3$: 99.9%, Wako), scandia (Sc_2O_3: 99.9%, Daiichi Kigenso) and zirconia (ZrO_2: 99.97% including 2 mass% of hafnia (HfO_2), Daiichi Kigenso). We assumed that the impurity hafnia does not influence the phase relationship in this system because the chemical properties of hafnium are quite similar to those of zirconium. All samples were finally heat-treated in the form of pellet at 1600 °C for 24 h in air. Flow charts of the synthesis procedures of samples are shown in Figs. 2(a) and (b) where the main difference is whether samples are embedded in the powder of the sample compositions or not, and the cooling method: (a) samples were heat-treated in the powder bed to suppress evaporation of BaO during heat treatment at 1600 °C because of relatively high vapor pressure of BaO at 1600 °C [3], and the samples were furnace-cooled; or (b) samples were heat-treated without a powder bed, and then quenched from 1600 °C to room temperature. In the latter case, we mechanically polished out the surface of the pellet and then employed the XRD and EDX analysis.

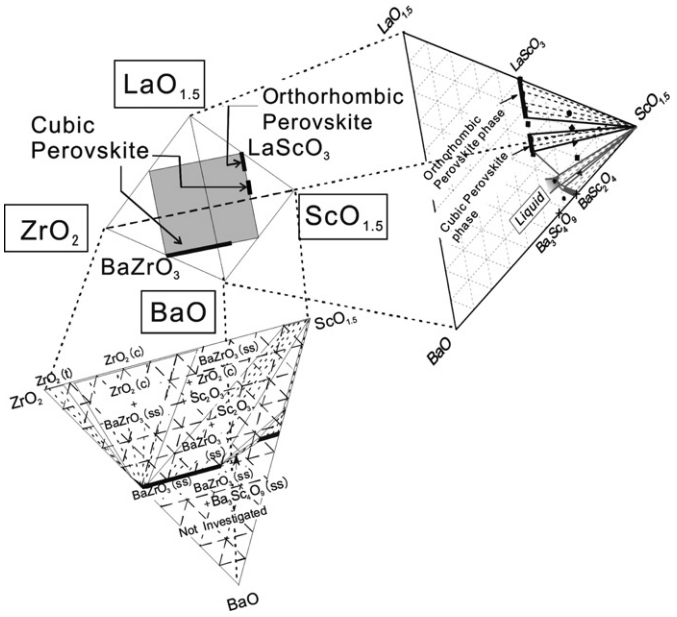

Fig. 1. Schematic pseudoquaternary phase diagram with two pseudoternary phase diagrams at 1600 °C.

3. Results and discussion

3.1. $LaO_{1.5}$–BaO–$ScO_{1.5}$ pseudoternary system at 1600 °C

We first established the pseudoternary phase diagram of the $LaO_{1.5}$–BaO–$ScO_{1.5}$ system at 1600 °C. The results are shown in Fig. 3, and the logistics and the detailed experimental results are explained below. In addition, it is noted that we utilized information of pseudobinary phase diagrams of a $LaO_{1.5}$–$ScO_{1.5}$ [4], BaO–$ScO_{1.5}$ [5] and BaO–$LaO_{1.5}$ [6] to establish this pseudoternary phase diagram. We just introduce the known phase, melting points and eutectic reaction under 1600 °C in the pseudobinary systems; the known phases are $LaO_{1.5}$ (m.p. 2304 °C), $ScO_{1.5}$ (m.p. 2300 °C), BaO (m.p. 1923 °C), $LaScO_3$, $BaSc_2O_4$ (m.p. 2100 °C), $Ba_3Sc_4O_9$ (m.p. 2050 °C) and $Ba_2Sc_2O_5$ (decomposition at 1000 °C). There is eutectic reaction at BaO–30 mass% $LaO_{1.5}$ at 1548 °C in the pseudobinary system of BaO–$LaO_{1.5}$.

Table 1
Nominal compositions of samples and phases identified by X-ray diffraction in samples heat-treated at 1600 °C for 24 h in air
(a) $LaO_{1.5}$–BaO–$ScO_{1.5}$ system

Sample	Nominal composition			Identified phase by XRD (○: detected, ×: undetected and –: Not examined)				
	$X_{ScO_{1.5}}$	X_{BaO}	$X_{LaO_{1.5}}$	$LaScO_3$ (orthorhombic)	$LaScO_3$ (cubic)	$ScO_{1.5}$	$BaSc_2O_4$	Unknown phase
T50[a]	0.50	0	0.50	○	×	×	×	×
T51[a]	0.50	0.05	0.45	○	×	×	×	×
T52[a]	0.50	0.10	0.40	○	×	×	×	×
T53[a]	0.50	0.15	0.35	○	○	×	×	×
T54[a]	0.50	0.20	0.30	×	○	×	×	×
T55[a]	0.50	0.25	0.25	×	○	×	×	○
T71[a]	0.70	0.05	0.25	○	×	○	×	×
T72[a]	0.70	0.10	0.20	○	○	○	×	×
T73[a]	0.70	0.15	0.15	×	○	○	×	○
T74[a]	0.70	0.20	0.10	×	○	○	×	○
T75[a]	0.70	0.25	0.05	×	×	○	○	○
Q[a]	0.575	0.325	0.1	–	–	–	–	–

(b) $LaO_{1.5}$–BaO–$ScO_{1.5}$–ZrO_2 system

Sample	Nominal composition				Identified phase by XRD (○: detected, ×: undetected and –: Not examined)		
	$X_{ScO_{1.5}}$	X_{BaO}	$X_{LaO_{1.5}}$	X_{ZrO_2}	$LaScO_3$ (orthorhombic)	$LaScO_3$ (cubic)	$Ba_3Sc_4O_9$
A0[a]	0.2875	0.2125	0.2875	0.2125	×	○	×
B0[a]	0.2125	0.2875	0.2125	0.2875	×	○	×
C0[a]	0.1375	0.3625	0.1375	0.3625	×	○	×

Table 1 (*continued*)

(b) $LaO_{1.5}$–BaO–$ScO_{1.5}$–ZrO_2 system

Sample	Nominal composition				Identified phase by XRD (○: detected, ×: undetected and –: Not examined)		
	$X_{ScO_{1.5}}$	X_{BaO}	$X_{LaO_{1.5}}$	X_{ZrO_2}	$LaScO_3$ (orthorhombic)	$LaScO_3$ (cubic)	$Ba_3Sc_4O_9$
D0[a]	0.0625	0.4375	0.0625	0.4375	×	○	×
A1[b]	0.3625	0.2125	0.2875	0.1375	×	○	×
B1[b]	0.2875	0.2875	0.2125	0.2125	×	○	×
C1[b]	0.2125	0.3625	0.1375	0.2875	×	○	×
D1[b]	0.1375	0.4375	0.1375	0.3625	×	○	×
A2[b]	0.4375	0.2125	0.2875	0.0625	×	○	×
B2[b]	0.3625	0.2875	0.2125	0.1375	×	○	×
C2[b]	0.2875	0.3625	0.1375	0.2125	×	○	×
D2[b]	0.2125	0.4375	0.0625	0.2875	×	○	×
B3[b]	0.4125	0.2875	0.2125	0.0875	×	○	×
C3[b]	0.3375	0.3625	0.1375	0.1625	×	○	×
D3[b]	0.2625	0.4375	0.0625	0.2375	×	○	×
P[a]	0.4000	0.4000	0.1000	0.1000	×	○	○
W0[a]	0.4375	0.0625	0.4375	0.0625	–	–	–
W1[a]	0.4375	0.0875	0.4125	0.0625	○	×	×
W2[a]	0.4375	0.1375	0.3625	0.0625	○	○	×

[a] Samples were quenched (by method in Fig. 2(b))
[b] Samples were furnace-cooled (by method in Fig. 2(a)).

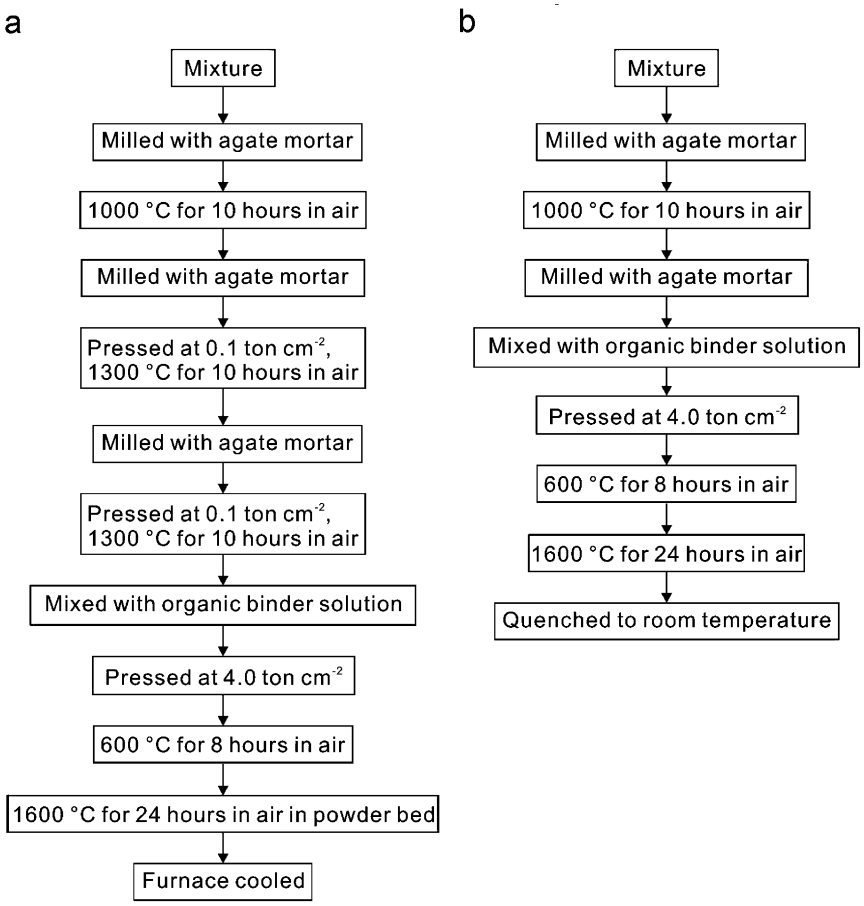

Fig. 2. Synthesis procedures of samples: (a) samples were heat-treated in the powder bed, and furnace-cooled, and (b) samples were heat-treated without a powder bed, and quenched from 1600 °C to room temperature.

3.1.1. Analysis of X-ray diffraction of samples of $X_{ScO_{1.5}} = 0.50$

Samples on the composition line of $X_{ScO_{1.5}} = 0.50$ were heat-treated at 1600 °C for 24 h. XRD patterns of the samples are shown in Figs. 4(a) and (b) and the identified phases are summarized in Table 1(a). Orthorhombic lanthanum scandate phase was identified in the samples of T50, T51, T52 and T53. When $X_{BaO} =$ 0.20 (T54), only cubic lanthanum scandate phase was identified. In the case of sample T53, the peak profile coincided with a

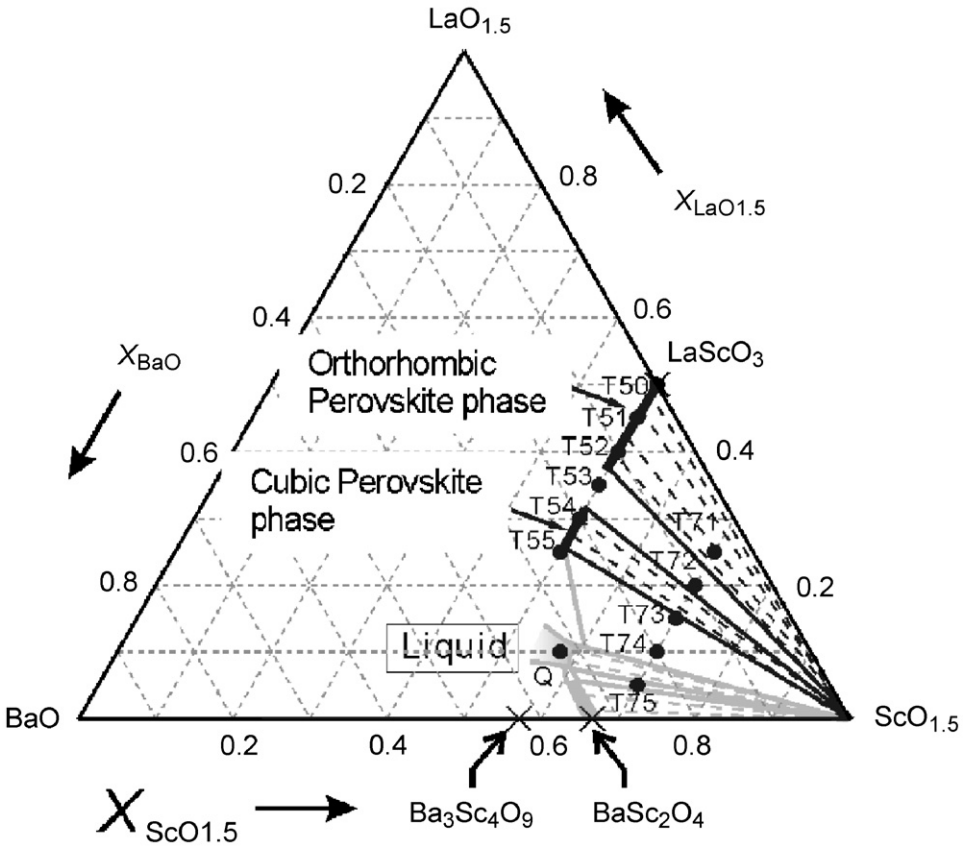

Fig. 3. Established pseudoternary phase diagram of the $LaO_{1.5}$–BaO–$ScO_{1.5}$ system at 1600 °C.

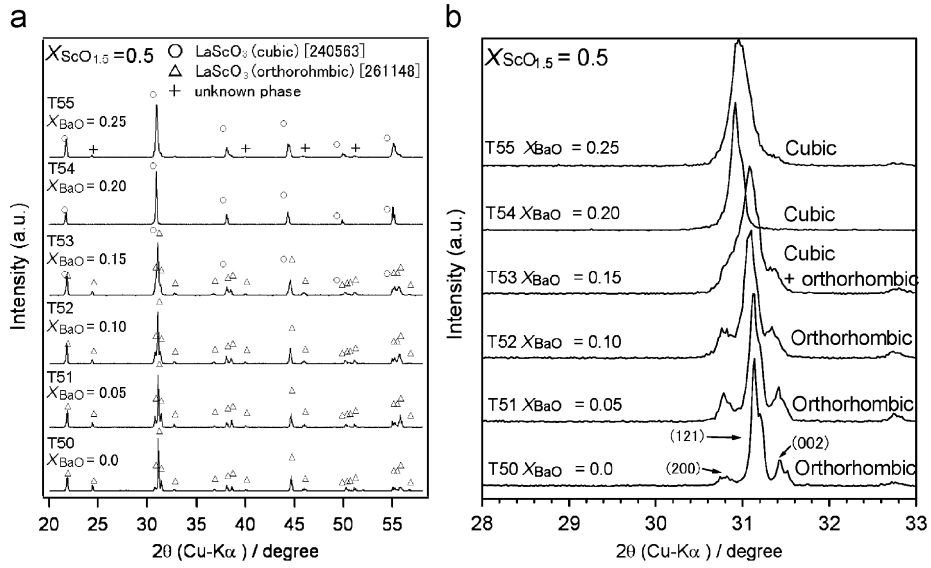

Fig. 4. XRD patterns of samples on the composition line of $X_{ScO_{1.5}} = 0.50$ (T50, T51, T52, T53, T54 and T55) after heat treatment at 1600 °C for 24 h. (a) 2θ from 20° to 58° and (b) 2θ from 28° to 33°.

superimposed diffraction profile of the orthorhombic lanthanum scandate phase (T52) and the cubic lanthanum scandate phase (T54) in the ratio of 0.8:0.2. Thus, we assumed that the sample T53 contains the orthorhombic and the cubic lanthanum scandate phase with such a ratio. When $X_{BaO} = 0.25$ (T55), cubic lanthanum scandate phase and unknown diffraction patterns were identified.

A discrepancy in phase identification with literature was recognized at T51 and T52. In Ref. [7], samples having the same composition of T51 and T52 were identified as mixture of cubic and orthorhombic phase but we could not see any evidence as mixture in T51 and T52. The main differences in processing seem to be synthesizing temperature and sintering period. We combined synthesizing and sintering process, that is, the samples was heat-treated at 1000 °C for 10 h and 1600 °C for 24 h. As the heat treatment at 1000 °C is not enough to synthesize lanthanum scandate phase, we can see un-reacted phases by XRD. But there is

Table 2
Compositions of each phase in samples heat-treated at 1600 °C for 24 h in air on a pseudoternary phase diagram of the $LaO_{1.5}$–BaO–$ScO_{1.5}$ system

	Nominal			$LaScO_3$ (orthorhombic)			$LaScO_3$ (cubic)			Sc_2O_3			$BaSc_2O_4$			Unknown phase		
	$X_{ScO_{1.5}}$	X_{BaO}	$X_{LaO_{1.5}}$	$X_{ScO_{1.5}}$	X_{BaO}	$X_{LaO_{1.5}}$	$X_{ScO_{1.5}}$	X_{BaO}	$X_{LaO_{1.5}}$	$X_{ScO_{1.5}}$	X_{BaO}	$X_{LaO_{1.5}}$	$X_{ScO_{1.5}}$	X_{BaO}	$X_{LaO_{1.5}}$	$X_{ScO_{1.5}}$	X_{BaO}	$X_{LaO_{1.5}}$
T53[a]	0.5	0.15	0.35	0.47	0.16	0.37	0.49	0.20	0.32	(n.d.)			(n.d.)			(n.d.)		
T54[a]	0.5	0.20	0.30	(n.d.)			0.50	0.20	0.29	(n.d.)			(n.d.)			(n.d.)		
T55[a]	0.5	0.25	0.25	(n.d.)			0.50	0.24	0.26	(n.d.)			(n.d.)			0.43	0.37	0.20
T71[a]	0.7	0.05	0.25	0.54	0.09	0.38	(n.d.)			0.98	0	0.02	(n.d.)			(n.d.)		
T72[a]	0.7	0.10	0.20	0.48	0.14	0.37	0.51	0.18	0.31	0.96	0.01	0.02	(n.d.)			(n.d.)		
T73[a]	0.7	0.15	0.15	(n.d.)			0.52	0.25	0.24	0.99	0	0	(n.d.)			0.44	0.36	0.2
T74[a]	0.7	0.20	0.10	(n.d.)			0.53	0.26	0.21	0.97	0.01	0.01	(n.d.)			0.60	0.29	0.11
T75[a]	0.7	0.25	0.05	0.50	0.20	0.29	(n.d.)			0.99	0	0	0.61	0.34	0.05	0.74	0.21	0.05

[a] Samples were quenched (by method in Fig. 3(b)).

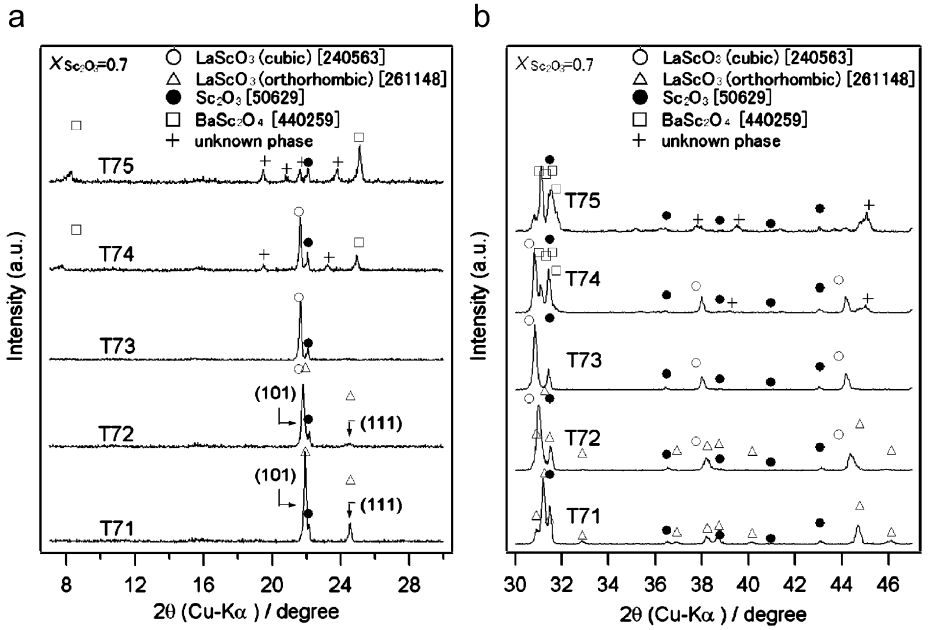

Fig. 5. XRD patterns of samples on the composition line of $X_{ScO_{1.5}} = 0.70$ (T71, T72, T73, T74 and T75) after heat treatment at 1600 °C for 24 h. (a) 2θ from 7° to 33°, and (b) 2θ from 30° to 47°.

no such phases after heat treatment at 1600 °C. In contrast, they synthesized by heating at 1500 °C for 5 h and sintered at 1600 °C for 10 h. We speculate that it is difficult to obtain the equilibrium phase relationship in their process if the phase relationship is different at between 1500 and 1600 °C. That is, it may take time for samples to reach equilibrium at 1600 °C after an achievement of equilibrium phase relationship at 1500 °C because grain growth is expected at 1500 °C. This phenomenon was recognized in barium zirconate previously [8].

3.1.2. Results of EDX analysis of samples of $X_{ScO_{1.5}} = 0.50$

Table 2 shows the average compositions, analyzed by EDX, of each grain in the samples heat-treated at 1600 °C for 24 h in air. Since there is a complete overlap between fluorescence X-rays of Ba Lα_1 and Sc Kβ_1, we subtracted the intensity of Sc Kβ_1 by using the calculated intensity of Sc Kβ_1 from the observed intensity of Sc Kα_1. We also subtracted relatively small overlap by the fluorescence X-rays of La Lα_1. We think EDX result is reliable for usage in this study. But, when the mole fraction of barium oxide is low, the compositions obtained by EDX were not so accurate. Thus we did not list the compositions of samples at $X_{BaO} = 0$, 0.05 and 0.10 (T50, T51 and T52) on Table 2 although there is no large dispersion in the analyzed compositions of grains in each sample (T50, T51 and T52). We consider the samples at $X_{BaO} = 0$, 0.05 and 0.10 (T50, T51 and T52) to be single phase.

It was confirmed that all analyzed grains of the lanthanum scandate phase in the sample at $X_{BaO} = 0.2$ (T54) had the same compositions as the average compositions. Thus, the sample at $X_{BaO} = 0.2$ (T54) is also single phase. At $X_{BaO} = 0.15$ (T53), there are two kinds of grains which had different compositions as shown in Table 2. This coincides with the results by XRD analysis where the sample T53 is in the two phase region of orthorhombic lanthanum scandate and cubic lanthanum scandate. At $X_{BaO} = 0.25$ (T55), two kinds of grains were observed. This also coincides with XRD identification of an unknown phase observed in addition to cubic lanthanum phase. The mole fraction of barium oxide in the cubic lanthanum scandate phase of the sample at $X_{BaO} = 0.25$ (T55) was 0.24. Thus, the solubility of barium into lanthanum scandate phase was determined to be $X_{BaO} = 0.24$ at 1600 °C.

3.1.3. Analysis of X-ray diffraction and EDX analysis of samples of $X_{ScO_{1.5}} = 0.70$

Figs. 5(a) and (b) shows XRD patterns of samples at $X_{ScO_{1.5}} = 0.70$ heat-treated at 1600 °C for 24 h. Combining the results obtained at $X_{ScO_{1.5}} = 0.50$, the phases in the samples were

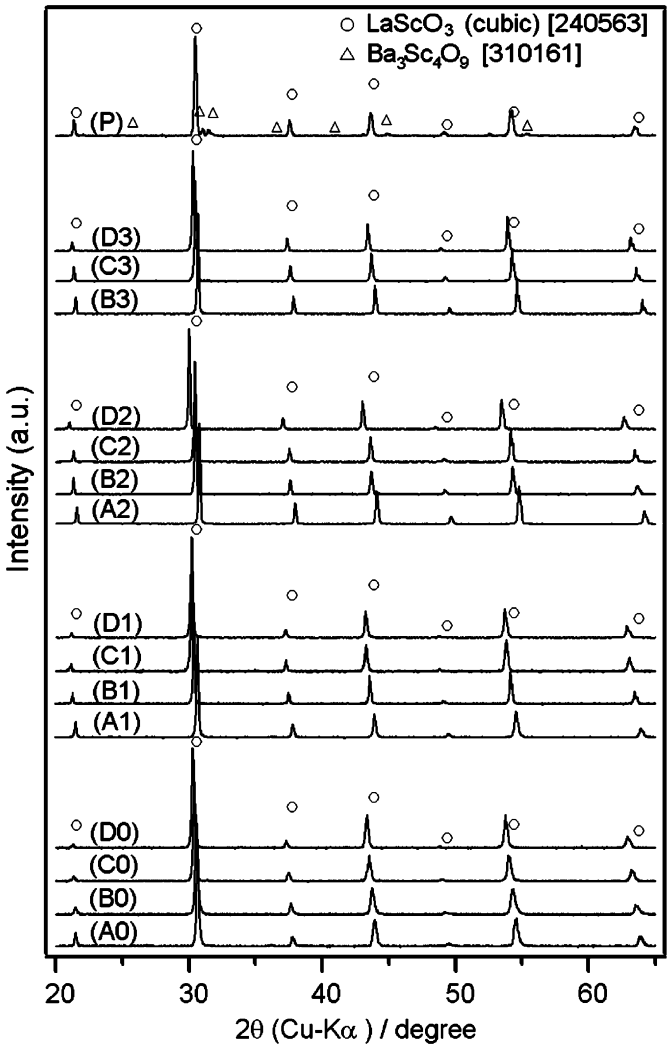

Fig. 6. XRD patterns of the samples (A0 to D0, A1 to D1, A2 to D2, B3 to D3 and P) after heat treatment at 1600 °C for 24 h.

identified as listed in Table 1(a). In all the samples (T71–T75), the scandia phase was detected. When the mole fraction of barium oxide was 0.05 ($X_{BaO} = 0.05$ (T71)), only orthorhombic lanthanum scandate phase was identified in addition to scandia phase. When $X_{BaO} = 0.10$ (T72), we assumed that both orthorhombic and cubic lanthanum scandate phase existed. We distinguished cubic lanthanum scandate from orthorhombic lanthanum scandate by the ratio of intensity of (101) to (111) because the diffraction at (111) is unique for the orthorhombic phase. When $X_{BaO} = 0.15$ (T73), cubic lanthanum scandate phase and scandia phase were detected. When $X_{BaO} = 0.20$ (T74), $BaSc_2O_4$ and unknown phase were detected in addition to cubic lanthanum scandate and scandia phase. The existence of four phases violates Gibbs' phase rule. We assumed that the existence of liquid phase at 1600 °C, decomposing to two or more phases on cooling. To confirm this assumption, we prepared sample Q which has a composition as indicated in Fig. 1(a) and Table 1(a), and then heat-treated at 1600 °C for 24 h. After heat treatment, the sample was completely melted. This indicates the possibility of a three-phase equilibrium containing liquid phase in the sample T74. In the sample T75 ($X_{BaO} = 0.25$), scandia, $BaSc_2O_4$ and unknown phase were identified. The peak positions of the $BaSc_2O_4$ phase shifted to lower angles than those in the JCPDS card [no. 440259, lattice constant, $a = 0.98341$ nm, $b = 0.58159$ nm, $c = 2.0578$ nm]. Thus, there is a possibility that $BaSc_2O_4$ has some solubility of lanthanum. The average compositions of grains in series of $X_{ScO_{1.5}} = 0.70$ are shown in Table 2. We expect that the composition of the liquid phase might be close to the four unknown phases in T55, T73, T74 and T75.

3.2. $LaO_{1.5}$–BaO–$ScO_{1.5}$–ZrO_2 pseudoquaternary system at 1600 °C

3.2.1. Analysis of X-ray diffraction of samples of A0 to D0, A1 to D1, A2 to D2, B3 to D3 and P

Samples (A0 to D0, A1 to D1, A2 to D2, B3 to D3 and P) on the composition plane between $LaScO_3$ and sum of 1/4 $Ba_3Sc_4O_9$ and 1/4 BaO, and $BaZrO_3$ and $La_2Zr_2O_7$ were heat-treated at 1600 °C for 24 h. XRD patterns of the samples (A0 to D0, A1 to D1, A2 to D2, B3 to D3 and P) are shown in Fig. 6. The identified phases are

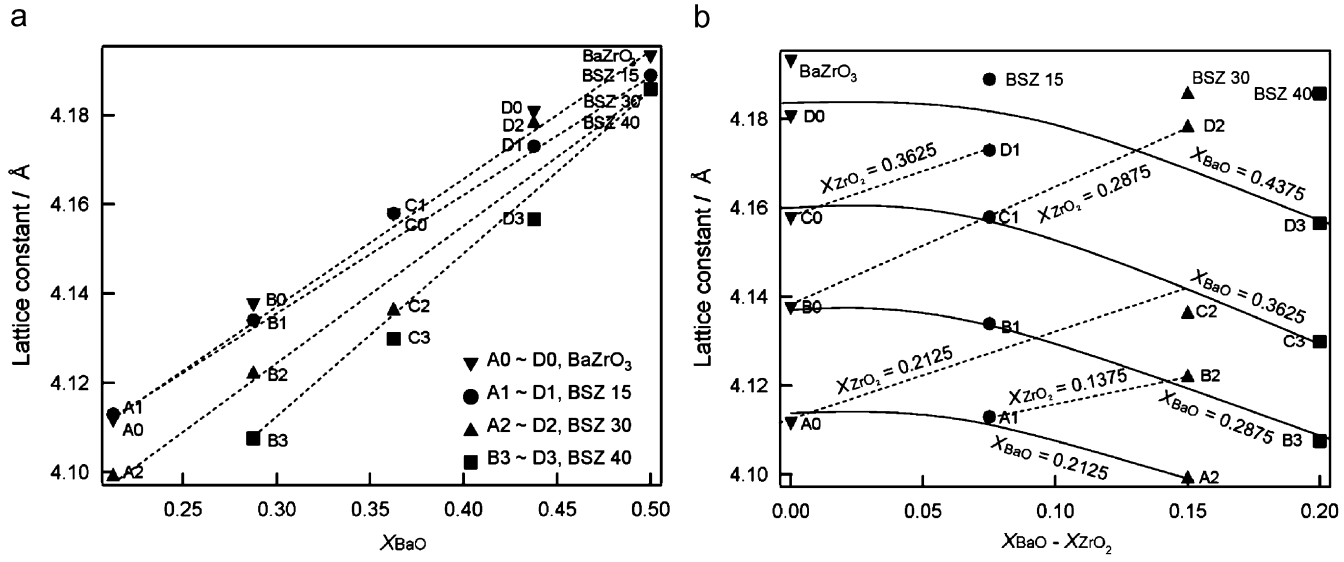

Fig. 7. Lattice constants of the samples (A0 to D0, A1 to D1, A2 to D2, B3 to D3, $BaZrO_3$, $BaZr_{0.85}Sc_{0.15}O_{3-\delta}$ (BSZ 15, $X_{ScO_{1.5}} = 0.075$), $BaZr_{0.7}Sc_{0.3}O_{3-\delta}$ (BSZ 30, $X_{ScO_{1.5}} = 0.15$) and $BaZr_{0.6}Sc_{0.4}O_{3-\delta}$ (BSZ 40, $X_{ScO_{1.5}} = 0.20$)) after heat treatment at 1600 °C for 24 h (a) as a function of X_{BaO}, and (b) as a function of $X_{BaO} - X_{ZrO_2}$.

summarized in Table 1(b). Only cubic perovskite phase was identified in all samples except for sample P. Figs. 7(a) and (b) shows lattice constants of cubic phases as a function of X_{BaO} and $X_{BaO}-X_{ZrO_2}$, respectively. The $X_{BaO}-X_{ZrO_2}$ corresponds to the concentration of oxygen vacancy in the electroneutrality condition. The lattice constants of $BaZrO_3$, $BaZr_{0.85}Sc_{0.15}O_{3-\delta}$ (BSZ 15, $ScO_{1.5}=0.075$), $BaZr_{0.7}Sc_{0.3}O_{3-\delta}$ (BSZ 30, $ScO_{1.5}=0.15$) and $BaZr_{0.6}Sc_{0.4}O_{3-\delta}$(BSZ 40, $ScO_{1.5}=0.20$) were also plotted in the figure for reference. Now, the ionic radius of barium is larger than that of lanthanum; Ba = 1.61 Å (12 coordination) and La = 1.36 Å (12 coordination). In contrast, the ionic radii of zirconium and scandium are almost the same; Zr = 0.72 Å (6 coordination) and Sc = 0.76 Å (6 coordination). In the algebraic sense, the lattice constant increases with increase of X_{BaO} which can be confirmed in Fig. 7(a). There is an almost linear relationship between X_{BaO} and the lattice constant except for D2 which might include some experimental error. Looking in further detail, we can find the lattice shrinking at high oxygen vacancy at the same X_{BaO} level as indicated with a solid line in Fig. 7(b). We suppose there might be some mechanism to relax a high energy state of the lattice caused by a high concentration of oxygen vacancy, such as formation of cation pair or ordering of oxygen vacancies. In sample P, the peak patterns of cubic lanthanum scandate and $Ba_3Sc_4O_9$ phase were identified by XRD analysis, as shown in Fig. 6. Therefore, it was determined that the phase boundary of cubic perovskite should be between the sample P and the line whose oxygen vacancy composition is 0.2. This phase boundary coincides with results of XRD in Ref. [9].

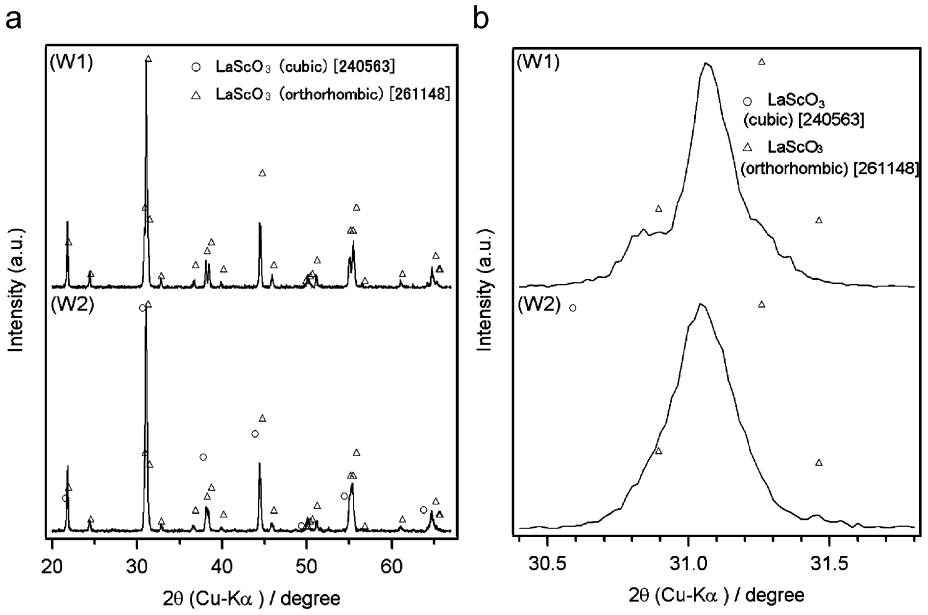

Fig. 8. XRD patterns of samples of W1 and W2 after heat treatment at 1600 °C for 24 h. (a) 2θ from 20° to 67°, (b) 2θ from 30.4° to 31.8°.

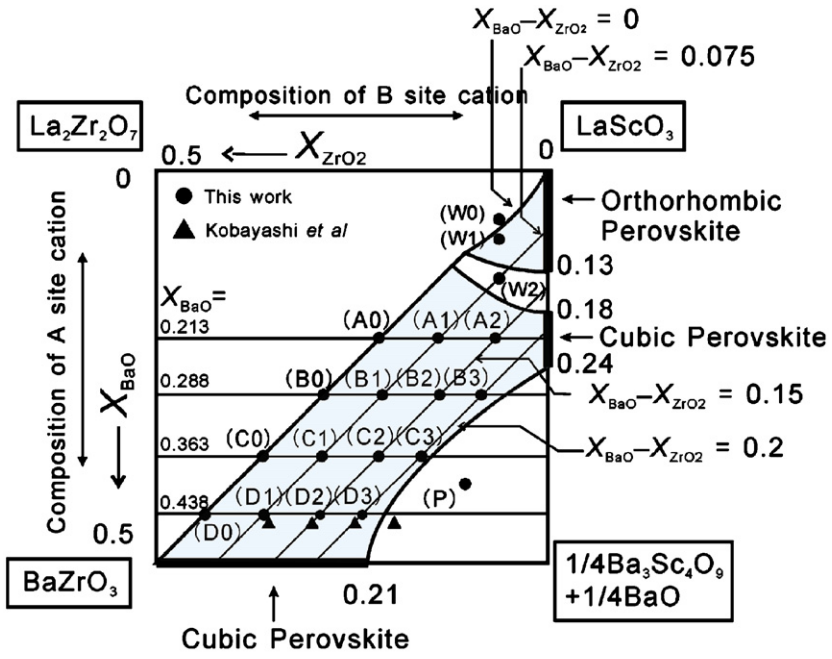

Fig. 9. A partial pseudoquaternary phase diagram of the $LaO_{1.5}$–BaO–$ScO_{1.5}$–ZrO_2 system at 1600 °C.

3.2.2. Analysis of X-ray diffraction and EDX in W0, W1 and W2

W0, W1 and W2 were prepared to establish the composition region of orthorhombic perovskite phases. The nominal compositions are listed in Table 1(b). Figs. 8(a) and (b) shows XRD patterns of samples of W1 and W2 after heat treatment at 1600 °C for 24 h and the phases are identified as summarized in Table 1(b). We employed the EDX for sample W2, and confirmed two types of grains in W2. The diffraction peaks of sample W2 look like cubic perovskite (Fig. 8(b)) but some unique diffraction peaks for orthorhombic phases were observed (Fig. 8(a)). Combining the results of EDX and XRD, we determine that sample W2 has two phases, and W1 is in the orthorhombic region. The shifts of peak positions from JCPDS card might be due to dissolution of barium and zirconium. Thus, the phase boundary of orthorhombic perovskite phase exists between samples W1 and W2. At the composition of sample W0, the sample melted during heat treatment at 1600 °C. This suggests that there is a liquid phase around sample W0.

We drew a partial pseudoquaternary phase diagram of the $LaO_{1.5}$–BaO–$ScO_{1.5}$–ZrO_2 system at 1600 °C based on information as obtained above, as shown in Fig. 9. In Fig. 9, the horizontal axis is composition of B site, X_{ZrO_2}, and vertical axis is composition of A site, X_{BaO}. The diagonal lines represent the same oxygen vacancy levels, that is $X_{BaO}-X_{ZrO_2}$. Now, keeping $X_{BaO}+X_{LaO_{1.5}}=0.5$ and $X_{ZrO_2}+X_{ScO_{1.5}}=0.5$, the difference between X_{BaO} and X_{ZrO_2} is equal to the concentration of oxygen vacancy with the assumption of holding electroneutrality. According to the established phase diagram, we can find that the solid solution of the cubic perovskite phase exists in the wide composition region.

4. Conclusions

The results obtained in this work can be summarized as follows:

(1) A part of the pseudoternary phase diagram of the $LaO_{1.5}$–BaO–$ScO_{1.5}$ system at 1600 °C was established. According to the phase diagram, the solubility of barium into lanthanum scandate is $X_{BaO}=0.24$ on the composition line where the mole fraction of scandium oxide is 0.50 ($X_{ScO_{1.5}}=0.50$).

(2) The phase boundary of solid solution between lanthanum scandate and barium zirconate at 1600 °C was clarified by establishing a partial pseudoquaternary phase diagram of the $LaO_{1.5}$–BaO–$ScO_{1.5}$–ZrO_2 system at 1600 °C. The cubic perovskite phase exists in a wide region. A symptom of partial ordering or formation of cation pair was suggested from the trend of lattice constants at high concentrations of oxygen vacancy.

Acknowledgments

This study was supported by a Grant-in-Aid for Young Scientists (A) from the Ministry of Education, Culture, Sports, Science and Technology of Japan. We also express our deep acknowledgement to Daiichi Kigenso Kagaku Kogyo Co., Ltd. and Pacific Metals Co., Ltd. for the supply of zirconia powder and scandia powder, and Professors E. Matsubara and T. Ichitsubo for allowing us to use FE-SEM.

References

[1] S. Kim, K.H. Lee, H.L. Lee, Solid State Ionics 144 (2001) 109–115.
[2] S. Imashuku, T. Uda, T. Ichitsubo, E. Matsubara, Y. Awakura, J. Phase Equilib. 28 (2007) 517–522.
[3] I. Barin, Thermochemical Data of Pure Substances, third ed., VCH Verlagsgesellschaft mbH, 1995.
[4] S.J. Schneider, R.S. Roth, J.L. Waring, J. Res. Natl. Bur. Stand. Sect. A 65 (4) (1961) 345–374.
[5] L.M. Kovba, L.N. Lykova, M.V. Paromova, T.A. Kalinina, Dokl. Akad. Nauk SSSR 260 (4) (1981) 924–927 (in Russian).
[6] A. Auriol, G. Hauser, J.G. Wurm, Battelle Memorial Institute, Columbus, Ohio, Private Communication, 1961 (tentative results).
[7] K.H. Lee, H.L. Lee, S. Kim, H.L. Lee, Jpn J. Appl. Phys. 44 (2005) 5025–5029.
[8] S. Imashuku, T. Uda, Y. Awakura, Electrochemical and Solid-State Letters 10 (2007) B175–B178.
[9] T. Kobayashi, H. Watanabe, M. Hibino, T. Yao, Solid State Ionics 176 (2005) 2439–2443.